Mon. Not. R. Astron. Soc. **347,** 411–420 (2004)

The hard X-ray spectrum of the Seyfert galaxy IRAS 18325–5926: reflection from an ionized disc and variable iron K emission

K. Iwasawa,[1]★ J. C. Lee,[2]† A. J. Young,[3] C. S. Reynolds[3] and A. C. Fabian[1]

[1] *Institute of Astronomy, Madingley Road, Cambridge CB3 0HA*
[2] *Massachusetts Institute of Technology, Center for Space Research, 77 Massachusetts Avenue NE80, Cambridge MA 02139, USA*
[3] *Department of Astronomy, University of Maryland, College Park, MD20742, USA*

Accepted 2003 September 13. Received 2003 September 9; in original form 2003 June 13

ABSTRACT

We report our analysis of the X-ray spectra of the Seyfert galaxy IRAS 18325−5926 (= Fairall 49) obtained from various X-ray observatories prior to *XMM–Newton*, including new results from two *RXTE* and one *BeppoSAX* observations. A relatively steep continuum slope ($\Gamma \simeq 2.2$) in the 2–15 keV band is confirmed. The continuum spectrum observed with the *BeppoSAX* PDS shows a possible roll-over at energies above 30 keV, indicating a Comptonizing corona cooler than in other Seyfert nuclei. The X-ray spectrum above 2 keV is best explained with a model including reflection from a highly ionized disc with significant relativistic blurring. The iron Kα emission feature is then mainly due to Fe XXV. The seven recent observations show that the iron K emission flux appears to follow the continuum between the observations separated by a few months to years, although some exceptions suggest that the linestrength may be determined in a more complex way.

Key words: galaxies: individual: IRAS 18325−5926 – galaxies: Seyfert – X-rays: galaxies.

1 INTRODUCTION

It has been recognized for a while that reflection, possibly from an optically thick accretion disc, is present in the X-ray spectrum of type 1 Seyfert galaxies (Pounds et al. 1990; Matsuoka et al. 1990). The detection of broad iron lines (Tanaka et al. 1995; Nandra et al. 1997b) supported the idea that the X-ray reflection might occur at a few gravitational radii ($r_{\rm g} = GM/c^2$) of a central black hole, where relativistic effects distort the line profile greatly due to strong gravity operating there (e.g. Fabian et al. 1989; Kojima 1991; Laor 1991).

Most active galactic nuclei (AGN) with broad Fe Kα show their line emission peaking at ∼6.4 keV, suggesting that the reflecting medium is cold (Nandra et al. 1997b), although it is partly due to a narrow line produced from a distant cold matter in some objects (e.g. Yaqoob et al. 1996; Weaver & Reynolds 1998). While strong X-ray illumination could photoionize the disc significantly, expected spectral signatures, particularly high-ionization iron line emission, e.g. Fe XXV Kα at 6.7 keV (e.g. Matt, Fabian & Ross 1993), has rarely been observed in Seyfert galaxies. Some evidence for high-energy iron lines has been reported for high-luminosity quasi-stellar objects (QSOs) or AGN classified as narrow-line type 1 Seyfert galaxies (e.g. Nandra et al. 1997c; Comastri et al. 1998; Leighly 1999; Ballantyne, Iwasawa & Fabian 2001a; Vaughan et al. 2002).

Reflection spectra from highly ionized matter can be rich in spectral features (Ross & Fabian 1993; Ross, Fabian & Young 1999; Nayakshin, Kazanas & Kallman 2000; Ballantyne, Ross & Fabian 2001b). At high ionization states, reduction of photoelectric absorption within the reflecting matter in the soft X-ray band causes some spectral features other than an Fe Kα line to be detectable in the soft X-ray spectrum, the reflection component of which makes up a significant fraction. Compton scattering within the highly ionized surface is expected to have a significant effect on the appearance of reflection spectra (e.g. Nayakshin et al. 2000), which may be coupled with various conditions of the accretion disc and the illuminating source. Therefore, investigating not only the iron line but also the whole X-ray spectrum is important.

In the context of reflection from an accretion disc, the general lack of response of the iron line flux to the continuum in the well-studied Seyfert galaxy MCG-6-30-15 (Lee et al. 1999; Shih, Iwasawa & Fabian 2002; Fabian & Vaughan 2003) poses a problem to the simplest disc reflection picture (note, however, that the line does vary despite any correlation with the continuum being unclear: see Iwasawa et al. 1996b, 1999). Although a study of the line variability is limited to relatively bright AGN, there have been some reports on variations of the Fe Kα line in other Seyfert galaxies (NGC 7314, Yaqoob et al. 1996; NGC 3516, Nandra et al. 1997a; Turner et al. 2002; Mrk 841, Petrucci et al. 2002). To investigate line variability, especially a correlation with the continuum is of great importance in understanding the production of the emission line and reflection in AGN.

★E-mail: ki@ast.cam.ac.uk
†Chandra Fellow.

We report, in this paper, evidence for reflection from a highly ionized disc that probably occurs in a relativistic region around a black hole and variable iron line emission in the Seyfert galaxy IRAS 18325−5926, a brief summary of the properties of which is given below. Prior to the most recent *XMM–Newton* observation, there were six X-ray observations of IRAS 18325−5926 with *Ginga*, *ASCA*, *RXTE* and *BeppoSAX*, from which iron line data are available. Long-term variability between these observations and their hard X-ray spectrum are our main focus in this paper.

IRAS 18325−5926 (= Fairall 49) is one of the IRAS galaxies selected for its warm infrared colour (De Grijp et al. 1985) hosting a type 2 Seyfert nucleus (Carter 1984; Iwasawa et al. 1995). The host galaxy is probably of S0 type and has been identified with one of the X-ray bright Piccinotti AGN (Piccinotti et al. 1982) by Ward et al. (1988). The redshift of the galaxy is $z = 0.0198$. The X-ray source is moderately absorbed by a column density of $N_{\rm H} \sim 10^{22}$ cm^{-2} and is highly variable, indicating the presence of an obscured type 1 Seyfert nucleus. During a five-day *ASCA* observation in 1997, the X-ray emission appeared to show quasi-periodic modulations with intervals of approximately 16 h (Iwasawa et al. 1998). It is one of the earliest AGN found to have a broad iron Kα line (Iwasawa et al. 1996a), but for unknown reasons this galaxy has often been overlooked from sample studies of the iron line feature.

Some peculiarities in the X-ray spectrum of IRAS 18325−5926 have been noticed. The X-ray spectral slope measured with *Ginga* (2–18 keV) was $\Gamma \sim 2.2$, which is steeper than that of other type 1 Seyfert galaxies measured with *Ginga* ($\Gamma \simeq 1.8$, Nandra & Pounds 1994). No spectral flattening at high energies (above 10 keV), which is usually found in type 1 Seyfert nuclei and is considered to be due to reflection from cold matter, was found (Iwasawa et al. 1995; Smith & Done 1996). The profile of the broad iron Kα emission peaks at around 6.8 keV in the first *ASCA* spectrum taken in 1993 (Iwasawa et al. 1996a). The iron line has a relatively large equivalent width (EW), peaks at an energy higher than 6.4 keV and the lack of a high-energy hump suggests X-ray reflection occurring from highly ionized disc rather than a cold disc.

2 OBSERVATION AND DATA REDUCTION

The X-ray data used for the analysis in this paper were obtained from *Ginga*, *ASCA*, *RXTE* and *BeppoSAX*. The log of these observations together with a most recent *XMM–Newton* observation is summarized in Table 1. With the galaxy redshift $z = 0.0198$ and $H_0 = 70$ km s^{-1} Mpc^{-1}, the flux of 1×10^{11} erg cm^{-2} s^{-1} corresponds to a luminosity of $\approx 0.9 \times 10^{43}$ erg s^{-1}. Results from the *Ginga* and *ASCA* observations have been published previously (Awaki et al. 1991; Iwasawa et al. 1995, 1996a, 1998; Smith & Done 1996a). The *Ginga* LAC spectrum is the one analysed by Iwasawa et al. (1995). Details of the data reduction for the longer *ASCA* observation in 1997 can be found in Iwasawa et al. (1998). Results and details of the *XMM–Newton* observation will be published elsewhere (Iwasawa et al., in preparation).

Table 1. X-ray observations of IRAS 18325−5926. The observation date given in the first column (Epoch) is the starting date of the respective observation. The duration of each observation is given in hours. The exposure time of each observation is useful time left after data selection.

Epoch	Duration (h)	Satellite	Exposure (ks)	F(2–10 keV) (10^{-11} erg cm^{-2} s^{-1})
1989 May 17	11	*Ginga*	8.7	2.6
1993 Sep 11	28	*ASCA*	36	1.3
1997 Mar 27	139	*ASCA*	243	1.9
1997 Dec 25	61	*RXTE*	131	2.4
1998 Feb 21	67	*RXTE*	134	1.8
2000 Mar 31	75	*BeppoSAX*	115	2.0
2001 Mar 05	33	*XMM*	120	1.2

The *ASCA* data obtained from the shorter observation in 1993 (reported in Iwasawa et al. 1996a) have been reduced using the latest calibration. In this *ASCA* observation, because of the pointed position of the telescope, the source photons are spread over the four charge-coupled device (CCD) chips in the SIS detector, and a non-negligible fraction of the total photons were lost in the interchip gaps, which requires correction. Also, the useful exposure time of the SIS is shorter than that of the GIS. To avoid unnecessary complications, we only use the GIS data from this observation. As a result of the updated calibration, the averaged 2–10 keV flux is larger than that previously reported.

The duration of the observations ranges between 11 and 139 h. The spectral resolution in full width at half-maximum (FWHM) of the spectrometers at the Fe K band is approximately 1 keV for the *Ginga* LAC and *RXTE* PCA, ~500 eV for the *ASCA* GIS and *BeppoSAX* MECS, ~130 eV for the *ASCA* SIS (for the 1993 observation; ~250 eV for the 1997 observation due to detector degradation) and *XMM–Newton* pn camera. The mean 2–10 keV flux for each observation is given in Table 1. The lowest mean flux was recorded during the latest *XMM–Newton* observation in 2001, although the highest flux during the observation was twice as high as the mean value.

Data reduction of two previously unpublished *RXTE* and one *BeppoSAX* observations are described below.

2.1 *RXTE* PCA data

The two *RXTE* observations were carried out on 1997 December 25–27, and 1998 February 21–24. The energy spectra from the two *RXTE* observations were reduced as follows. The PCA spectra were extracted only from the top xenon layer using the FTOOLS 5.2 software. Data from all PCUs are combined, after weighting according to exposure to improve the signal-to-noise ratio.

Good time intervals were selected to ensure stable pointing, and exclude periods of South Atlantic Anomaly (SAA) passage. Elevation is restricted to be more than 10° above the Earth's limb. We also filter out electron contamination events. The net exposure times for the two PCA spectra are 131 ks for the 1997 December observation and 134 ks for the 1998 February observation.

We generate background data using PCABACKEST v3.0 in order to estimate the internal background caused by interactions between the radiation/particles and the detector/spacecraft at the time of observation. This is done by matching the conditions of observations with those in various model files. The model files used are the latest[1] 'CM' background models (a refinement of the L7-240 models) which are intended for application to faint sources with count rate less than 100 count s^{-1}. The PCA response matrix for the *RXTE* data set was created using PCARSP v8.0. Background models and response matrices are representative of the most up-to-date PCA calibrations.

Despite the improved background estimate, there are still features above 16 keV where the signal-to-noise ratio is low. The data analysed below are limited to the energy range of 3–16 keV.

---

[1] http://lheawww.gsfc.nasa.gov/users/craigm/pca-bkg/bkg-users.html

2.2 *BeppoSAX* data

IRAS 18325−5926 was observed with *BeppoSAX* during the period between 2000 March 31 and April 3. Spectral data are available from three detectors (LECS, MECS and PDS), which are sensitive and calibrated for a scientific analysis to X-rays in the energy ranges of 0.1–4, 2–10 and 14–200 keV, respectively. The event files for the MECS and LECS data were provided by the SAX Data Center (SDC). Events from the two MECS detectors (MECS2 and MECS3) have been merged and the MECS spectrum was extracted from the merged event file. The PDS spectrum, which has been reduced and corrected for background by SDC, is used for our analysis. The count rates in the respective detectors for net exposure times are 0.087 count s^{-1} for 39 ks (LECS), 0.23 count s^{-1} for 115 ks (MECS) and 0.13 count s^{-1} for 59 ks (PDS). The X-ray flux quoted is obtained from the MECS. The relative normalization ratio of the LECS to the MECS was found to be $\simeq$0.7 from fitting, while that of the PDS is fixed at 0.86 in the spectral analysis.

3 RESULTS

3.1 Light curves from *RXTE* and *BeppoSAX*

Light curves in the 2–10 keV band from the *RXTE* and *BeppoSAX* observations are shown in Fig. 1. The *RXTE* light curves are obtained from the five PCUs, while the *BeppoSAX* light curve is from the MECS. Although there is a hint of X-ray flux peaking every 40–50 ks during the *RXTE* 1998 observation, no significant periodic signals are found in these light curves, contrary to the nine cycles of 16-h quasi-periodic modulations found in the five-day long *ASCA* observation in 1997 (Iwasawa et al. 1998).

Count-rate ratios between three energy bands (2–4, 4–7 and 7–12 keV) have been examined, using the *RXTE* data. There are occasional deviations from the mean value but no correlated ratio changes with total flux were found. As a whole, the data are consistent with no variations in X-ray colour.

3.2 Steep spectral slope

An earlier measurement of the spectral slope for the 2–18 keV spectrum from the *Ginga* LAC indicated a relatively steep power-law slope ($\Gamma \sim 2.2$). No significant evidence for spectral hardening above 10 keV (Iwasawa et al. 1995; Smith & Done 1996), which are typically found in normal type 1 Seyfert galaxies (Nandra & Pounds 1994), was found. The spectra obtained from the *RXTE* PCA and the *BeppoSAX* MECS/PDS confirmed these results and revealed more spectral complexity. Here we discuss the *RXTE* and *BeppoSAX* spectra.

Fig. 2 shows plots of the ratios of the *RXTE* PCA spectra against an absorbed power law with photon index of $\Gamma = 2.0$ and an excess absorption column density above the Galactic value ($N_{\mathrm{H}} = 7.4 \times 10^{20}$ cm^{-2}, Dickey & Lockman 1990) $N_{\mathrm{H}} = 1 \times 10^{22}$ cm^{-2}. The normalization of the power law is adjusted so that the 3–5 keV range matches the 1998 February data. This absorbed power law was chosen only for the purpose of displaying spectral features.

It is clear from Fig. 2 that the continuum slopes of both spectra are steeper than $\Gamma = 2.0$. A naive estimate of a power-law slope for the continuum in the two respective spectra is $\Gamma \sim 2.2$, although a simple power-law fit even with a Gaussian for the Fe Kα does not provide a good agreement with the data due to more complex spectral features, as described in the following section. Fig. 2 also shows that the spectrum during the 1997 December observation is steeper than that during the 1998 February observation: the observed flux in the 1997 December data is brighter by ~40 per cent at 3 keV than the 1998 February data but only by ~20 per cent at 15 keV.

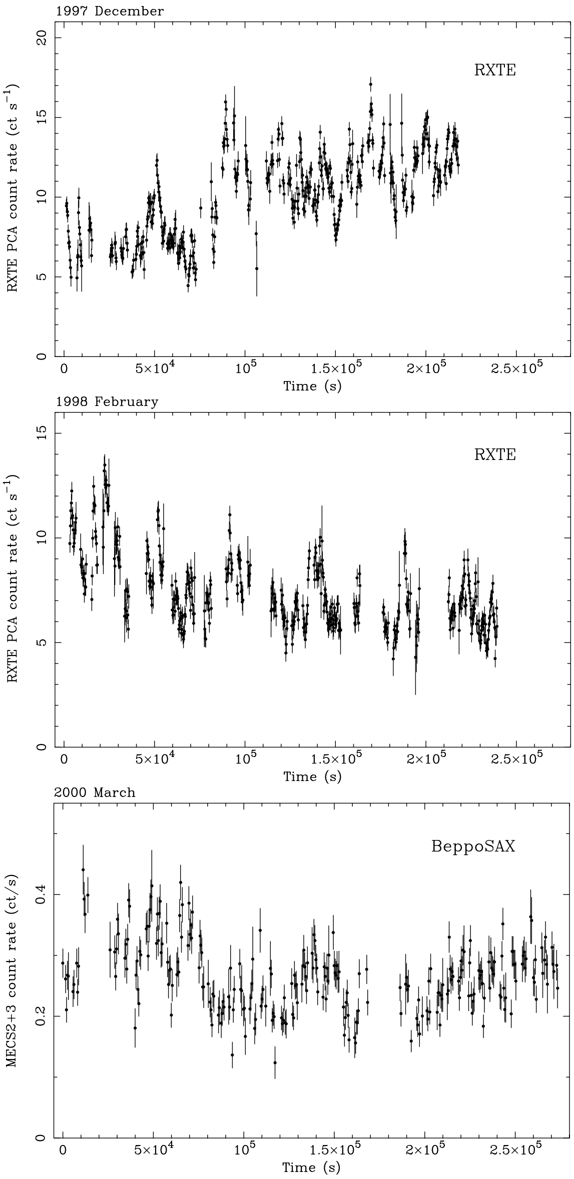

Figure 1. The 2–10 keV X-ray light curves of IRAS 18325−5926 during the two *RXTE* observations in 1997 and 1998 and the *BeppoSAX* observation in 1999.

3.3 Possible high-energy roll-over

The broad-band X-ray spectrum of IRAS 18325−5926 is investigated using data from the three detectors on board *BeppoSAX* (Fig. 3). As noted in the previous *ASCA* and *ROSAT* PSPC observations, there is an excess component below 1 keV, which appears to be less variable than the higher-energy emission (Iwasawa et al. 1996a). This has been confirmed with the longer *ASCA* observation. Although the origin of this soft excess component is unclear, we tentatively model this component using a partial covering absorber to a power law for describing the soft X-ray spectrum obtained from the *BeppoSAX* LECS.

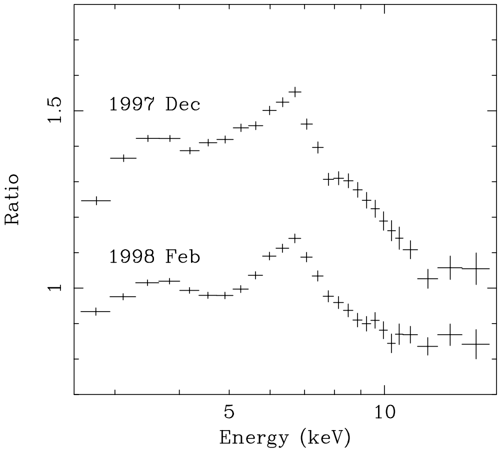

Figure 2. Plot of the ratio of the *RXTE* spectra taken in 1997 December and 1998 February to the absorbed power-law model with $\Gamma = 2$ and $N_{\mathrm{H}} = 1 \times 10^{22}$ cm^{-2}. The normalization of the power law is adjusted to match the 1998 February spectrum at around 3–5 keV. Spectral steepening and a significant edge-like feature above 10 keV are recognized in the 1997 December observation.

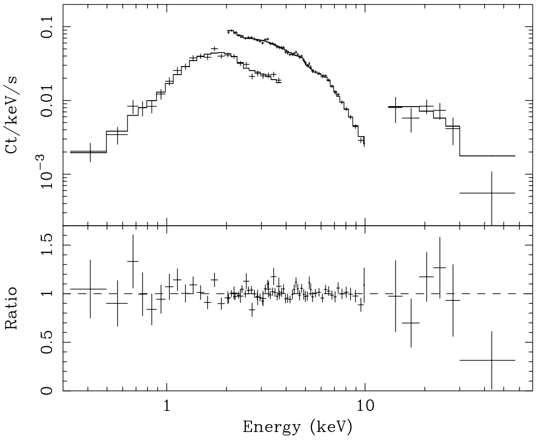

Figure 3. The *BeppoSAX* spectrum of IRAS 18325−5926. The LECS (0.3–4 keV), MECS (2–10 keV) and PDS (14–60 keV) data are plotted with the model (solid-line histogram) consisting of a power law and a Gaussian iron Kα line modified by a partially covering cold absorber at the galaxy's redshift and Galactic absorption that best fits the LECS and MECS data. Extrapolating the model to higher energies matches the PDS data up to 30 keV but overestimates significantly above that energy, as shown in the residual in the form of the ratio of the data and the model.

This partially absorbed power law plus a Gaussian for the Fe Kα emission provides a good fit to the MECS and LECS data in the 0.3–10 keV band with $\chi^2 = 110.5$ for 89 degrees of freedom. The Galactic absorption $N_{\mathrm{H}} = 7.4 \times 10^{20}$ cm^{-2} is included in the fit. Best-fitting spectral parameters for the continuum are $\Gamma = 2.13^{+0.06}_{-0.07}$, $N_{\mathrm{H}} = 1.3^{+0.1}_{-0.2} \times 10^{22}$ cm^{-2}, and the covering fraction of the absorber, $f_{\mathrm{C}} = 0.95^{+0.01}_{-0.01}$; hereafter errors quoted to spectral parameters are of the 90 per cent confidence limit for one parameter of interest unless stated otherwise.

Extrapolating this continuum model agrees with the PDS data up to 30 keV, but overestimates the data at energies above 30 keV. The PDS data above 50 keV are essentially at the noise level. The detected count rate in the 30–50 keV band are a factor of 4 ($\geqslant$1.8) below the extrapolation of the power-law continuum best fitting the MECS data, and its deviation is 2σ.

Apparently the high-energy roll-over is too steep to be an exponential cut-off [$\exp(-E/E_{\mathrm{c}})$, where E_{c} is a cut-off energy in keV] to the power law. It is better described by a sharp cut-off at 29^{+16}_{-15} keV with an e-folding energy of 6 keV [$\exp((E_{\mathrm{c}} - E)/E_{\mathrm{f}})$ for $E > E_{\mathrm{c}}$], which is, however, not constrained very well [$E_{\mathrm{f}} \leqslant 100$ keV]. Background subtraction at this high-energy end introduces an additional uncertainty, especially given the low count rate: a subtle oversubtraction of the instrumental line at around 50 keV in the background could cause a sharp decline in the source spectrum, such as that seen in our data. The HEXTE data from the *RXTE* observations do not have sufficient quality to provide any useful constraints on the spectral shape in this energy band. We therefore regard this high-energy deficit as a tentative detection of a spectral roll-over at 30 keV. This roll-over, however, would have little effect on the measurements of the strength of reflection using the data up to ∼20 keV such as *Ginga* LAC and *RXTE* PCA data.

As discussed in the following section, the X-ray spectrum can be explained by a model with reflection from an ionized disc. The reflection spectrum produces a spectral bump around 30 keV due to Compton down-scattering, which could partly explain the observed drop of X-ray flux above 30 keV (see e.g. Barrio, Done & Nayakshin 2003). As noted by e.g. Stern et al. (1995) and Petrucci et al. (2001), the temperature of the Comptonizing corona cannot necessarily be inferred from the energy of the power-law cut-off. We then fit the *BeppoSAX* data with the Comptonization model COMPPS by Poutanen & Svensson (1996), combined with the ionized reflection model XION by S. Nayakshin (the details of which will be described in Section 3.7). Note that the XION code assumes a power law with a high-energy cut-off as an illuminating source rather than the Comptonized continuum, which should, however, have little effect on the fit. The fittings were performed assuming either spherical or cylindrical geometries, which give similar quality of fit with a coronal temperature of $kT_{\mathrm{e}} = 35$–40 keV and optical depth of $\tau \simeq 2$. The statistical uncertainty of the derived temperature is the order of ±5 keV, but the systematic error mentioned above should dominate the uncertainty.

3.4 Emission lines and absorption edge

Here, we present a spectral analysis of the data from *Ginga*, *RXTE*, *BeppoSAX*, *ASCA* and *XMM–Newton*, using a simple phenomenological model. The fitted model consists of an absorbed power law and a Gaussian for the broad Fe Kα line. Results of spectral fits are shown in Table 2. Variability and correlations of some key spectral parameters will be discussed in the next subsection.

The 1997 December spectrum shows a significant deficit against a power law between 10 and 15 keV, the shape of which can be approximated by an absorption edge at $10.7^{+0.4}_{-0.4}$ keV with optical depth $\tau = 0.18^{+0.05}_{-0.06}$ (Fig. 2). No strong absorption edge is expected at this energy. An immediate interpretation of this feature is a blueshifted Fe K absorption edge, but an alternative origin of this feature is discussed in Section 3.7. Such an edge-like feature is not significantly detected in any other spectra (e.g. the 90 per cent upper limit on the optical depth of an absorption edge at the same energy in the 1998 February *RXTE* spectrum is $\tau \leqslant 0.12$).

In addition to the prominent Fe Kα emission, there is a weaker excess at ∼3.4 keV in the *RXTE* spectra (Fig. 2). This feature is also present in the *Ginga* LAC spectrum with lower signal-to-noise ratio and the good-quality *XMM–Newton* spectrum. It can be identified with the radiative recombination continuum (RRC) of S XVI in the

Table 2. Spectral fits to the *Ginga*, *RXTE*, *ASCA*, *BeppoSAX* and *XMM–Newton* pn spectra. The fitted model consists of an absorbed power law with a Gaussian for Fe Kα. The line centroid energy has been corrected for the galaxy redshift ($z = 0.0198$). It should be noted that the line centroid does not necessarily coincide with the peak of the emission-line profile when a skewed profile is fitted, particularly in a low-resolution spectrum, by a Gaussian, which has a symmetric shape.

Data	Band (keV)	Γ	$N_{\rm H}$ (10^{22} cm^{-2})	$E_{\rm Fe}$ (keV)	$\sigma_{\rm Fe}$ (keV)	$I_{\rm Fe}$ (10^{-5} photon s^{-1} cm^{-2})	$EW_{\rm Fe}$ (eV)	χ^2/d.o.f.
Ginga	2–18	$2.26^{+0.05}_{-0.06}$	$1.42^{+0.10}_{-0.21}$	$6.38^{+0.22}_{-0.12}$	$0.64^{+0.17}_{-0.23}$	$11.1^{+4.3}_{-3.1}$	411	14.16/21
*ASCA*93	2–10	$2.26^{+0.20}_{-0.15}$	$1.47^{+0.44}_{-0.38}$	$6.54^{+0.17}_{-0.20}$	$0.59^{+0.20}_{-0.19}$	$7.64^{+6.06}_{-2.38}$	626	422.1/418
*ASCA*97	2–10	$2.00^{+0.03}_{-0.05}$	$1.04^{+0.12}_{-0.12}$	$6.59^{+0.11}_{-0.11}$	$0.58^{+0.16}_{-0.17}$	$5.46^{+1.62}_{-1.53}$	268	1856.4/1802
*RXTE*97	3–16	$2.24^{+0.02}_{-0.03}$	$2.37^{+0.29}_{-0.29}$	$6.53^{+0.08}_{-0.09}$	$0.46^{+0.16}_{-0.10}$	$6.52^{+1.29}_{-1.07}$	244	74.00/30[a]
*RXTE*98	3–16	$2.17^{+0.03}_{-0.02}$	$1.62^{+0.29}_{-0.12}$	$6.65^{+0.07}_{-0.06}$	$0.41^{+0.16}_{-0.04}$	$5.58^{+1.40}_{-1.27}$	312	42.82/30
BeppoSAX	2–10	$2.19^{+0.11}_{-0.08}$	$1.52^{+0.22}_{-0.23}$	$6.50^{+0.24}_{-0.34}$	$0.42^{+0.88}_{-0.42}$	$4.47^{+8.13}_{-2.60}$	201	77.53/64
XMM	2–11	$2.06^{+0.03}_{-0.03}$	$1.24^{+0.08}_{-0.11}$	$6.61^{+0.07}_{-0.06}$	$0.43^{+0.04}_{-0.11}$	$2.99^{+0.43}_{-0.57}$	242	1119.0/1125

Notes. [a]The best-fitting spectral parameters given for the 1997 December RXTE spectrum are those obtained when an absorption edge is also included to describe the 10–15 keV deficit with $\chi^2 = 44.64$ for 28 degrees of freedom (see text for details), but the χ^2 value given in this table is for the fit without the edge model for a comparison with the other fits.

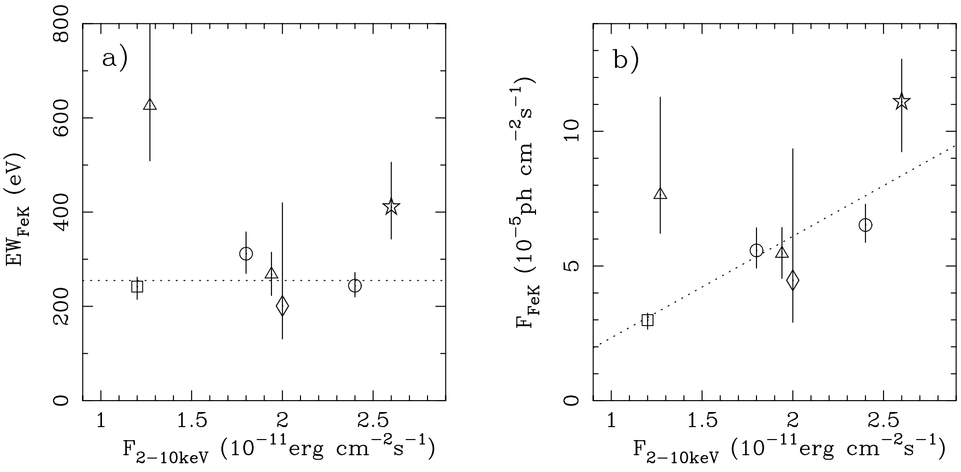

Figure 4. (a) Plot of equivalent width (EW) of the Fe Kα line, derived by fitting a Gaussian, against the 2–10 keV flux for the observations with *Ginga* (star), *ASCA* (triangles), *RXTE* (circles), *BeppoSAX* (diamond) and *XMM–Newton* (square). The dotted line shows a fit with a constant value ($\mathrm{EW_{FeK}} = 255^{+24}_{-22}$ eV) for the data except the *ASCA*93 observation with $\chi^2 = 4.9$ for five degrees of freedom. (b) Plot of Fe K line flux against the 2–10 keV flux; symbols represent the same observations as part (a). Error bars represent 1σ errors. The dotted line shows a linear correlation of $F_{\rm FeK} = -\,1.42^{+1.32}_{-1.32} + 3.67^{+0.89}_{-0.89} F_{\rm 2-10keV}$, where $F_{\rm FeK}$ and $F_{\rm 2-10keV}$ are the Fe Kα line flux and the 2–10 keV flux in the unit used in the plot ($\chi^2 = 5.2$ for four degrees of freedom). The fit excludes the data point from the *ASCA*93 observation.

context of the ionized reflection model discussed below. Although uncertainties in calibration of the detector response at the lowest energies are suspected for the *RXTE* PCA, since the excess is at 3σ level in the two *RXTE* spectra and the *XMM–Newton* spectrum has detected the same feature clearly (Iwasawa et al., in preparation), the presence of the feature is highly probable.

3.5 Variable iron K line emission

The 2–10 keV flux averaged over each observation was observed to vary by a factor of 3 between the seven observations analysed above (Table 1). Any response of the iron K line to the continuum is of great interest in the context of a reflection model for producing the iron line emission, although, with only seven data points, it is premature to discuss the reality of a correlation on statistical grounds.

Apart from the first *ASCA* observation in 1993 when the line EW is unusually large, a correlation between the line and continuum flux appears to exist (Fig. 4). Since there might be uncertainties in absolute flux calibration between the instruments, the EW of the lines, which are independent of the cross-calibration errors, are plotted against the measured 2–10 keV flux (see also Fig. 5) along with the plot of the line fluxes.[2] One could also claim that the line flux is continuously decreasing regardless of the continuum luminosity (Table 2).

The lineshape remains roughly the same between the observations. The means of the line centroid energy and linewidth are

---

[2] *ASCA* and *BeppoSAX* are in agreement within 3 per cent in absolute flux in a simultaneous observation of 3C 273 (*ASCA* GOF Calibration Memo 06/07/00). With the latest calibration, the *RXTE* measurement should be in a reasonable agreement (e.g. ∼10 per cent) with the above two, although fluctuation of the diffuse X-ray background (XRB) is a major uncertainty for an X-ray source with the brightness of IRAS 18325−5926. The *Ginga* flux is less affected by the XRB problem, because local background data were taken.

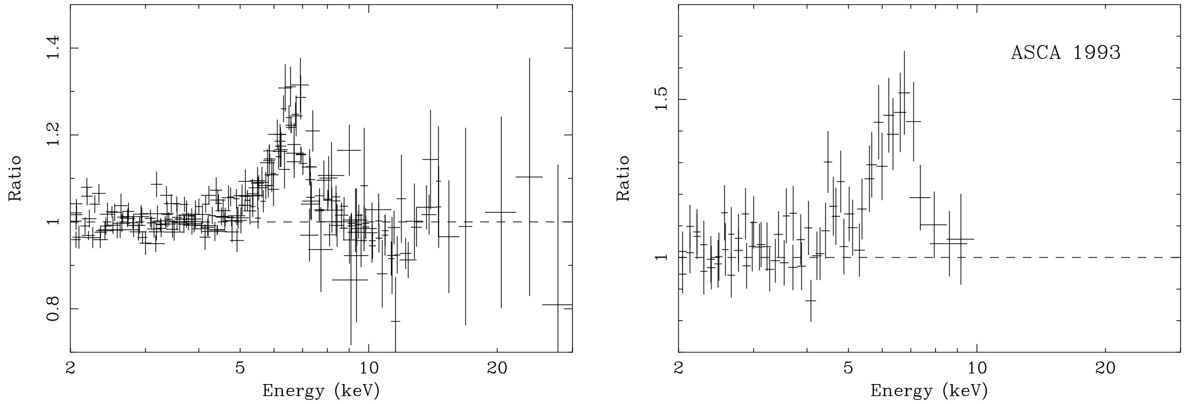

Figure 5. Left: The Fe Kα line profiles from all the observations except for the *ASCA*93 observation, which is plotted separately in the right panel, as a ratio relative to the respective best-fitting power-law continua. The data plotted here were obtained from detectors with a broad range of spectral resolution (from a proportional counter to an X-ray CCD). However, the measured linewidths (see Table 2) are comparable with the worst resolution of the proportional counters, which means that the overall shape of the lines can be compared regardless of the resolving power of the detector. Right: The same plot obtained from the *ASCA*93 observation (Iwasawa et al. 1996a). Note the difference in *y*-axis scale. The *ASCA*93 line is approximately twice as strong as the others.

6.59 keV and 0.47 keV (these values are weighted means). The iron lineshape in the form of a ratio against the best-fitting power-law continuum for all spectra is shown in Fig. 5.

3.6 Evidence for reflection from an ionized disc

One notable feature in the X-ray spectrum of IRAS 18325$-$5926 is the broad Fe Kα emission peaking at energies significantly higher than 6.4 keV, at which most Fe Kα lines of type 1 Seyfert galaxies are found (e.g. Nandra et al. 1997b). To interpret the iron line feature, reflection from a highly ionized disc is favoured for the following reasons.

The shape of the iron Kα line can be explained by broadened Fe XXV at 6.7 keV. A very high EW ($\sim$600 eV, see Table 2 and Iwasawa et al. 1996a) was observed in the spectrum of the *ASCA*93 observation. The high fluorescence yield of Fe XXV (Matt et al. 1993) can explain such a large EW. A bump at around 3.4 keV can be identified with the RRC of S XVI (Section 3.4), which is expected in a reflection spectrum with strong Fe XXV.

No significant high-energy hump above 10 keV is observed (Iwasawa et al. 1995; Smith & Done 1996). Compared to the case of cold reflection, in which a high-energy hump due to Compton down-scattering stands out when the incident power law and reflection spectrum are added (e.g. George & Fabian 1991), in ionized reflection, strong reflection takes place also at lower energies, where photons that entered and are reflected back into the ionized matter are no longer subject to photoelectric absorption, resulting in the Compton down-scattered hump being less pronounced because of a smaller contrast between low- and high-energy ranges (e.g. Ross & Fabian 1993).

A recent study of a photoionized disc in hydrostatic equilibrium by Nayakshin and collaborators (Nayakshin et al. 2000) predicts that AGN with a steep continuum slope ($\Gamma > 2$) tend to show distinctive 'ionized disc' signatures, e.g. strong Fe XXV plus Fe XXVI Kα emission, as predicted in the constant-density models (e.g. Ross & Fabian 1993; Ross et al. 1999; Ballantyne et al. 2001b). This is because the softer ionizing radiation causes the Compton temperature of the ionized surface of the disc to remain cool so that the region is not completely ionized. A low cut-off energy of the incident power law also helps for the same reason. These conditions fit the photon index ($\Gamma \simeq 2.2$, Section 3.2) and the possible spectral roll-over at 30 keV (Section 3.3) observed in IRAS 18325$-$5926.

3.7 Fitting the ionized reflection model

We have compared spectra expected from the ionized disc models with the observed X-ray spectra of IRAS 18325$-$5926. The presence of the S XVI RRC feature is in favour of using the reflection model from an ionized disc computed by XION, over the models by Ross & Fabian (1993) in which atomic features of sulphur have not been included.

The ionized reflection model gives good fits to all seven spectra. The iron line feature at 6–7 keV comprises multiple lines but is dominated by Fe XXV Kα at 6.7 keV in these models. The quality of the fits is comparable to or sometimes better than the phenomenological model with an absorbed power law and a Gaussian given in Table 2. The improvement in the ionized reflection fits comes from explaining the S XVI RRC feature around 3.4 keV in the high signal-to-noise ratio data from *Ginga* and *RXTE*.

Sharp spectral features like Fe Kα line are broadened to some degree via Compton scattering within the reflection layer when the disc is highly ionized. However, the broadening by Compton scattering is insufficient to explain the observed iron line profiles, and the data require significant relativistic broadening, expected for the region close to a central black hole.

This relativistically blurred ionized reflection can partly explain the puzzling edge-like feature at 10.6 keV in the 1997 December *RXTE* spectrum: broadened Fe XXV RRC, which would peak at 9.2 keV in the absence of relativistic broadening, makes a shoulder dropping at around 10 keV, mimicking an absorption edge at 10.5 keV (Fig. 6). However, a shallow deficit still remains. Introducing an extra absorption edge at $E_{\mathrm{th}} = 11.4^{+0.7}_{-0.7}$ keV with optical depth $\tau = 0.11$ improves the fit by $\Delta\chi^2 = 9.4$ from the fitting with the reflection model alone given in Table 3.

In order to make a comparison between the data sets easier, we restrict the number of free parameters to a minimum in the spectral fits. Apart from the photon index (Γ) of the illuminating power law, its normalization and cold absorption column density (N_{H}), only the luminosity ratio of the illuminating X-ray source and thermal emission from the disc, $l_{\mathrm{X}}/l_{\mathrm{d}}$, is allowed to vary where possible. This parameter basically defines the Compton temperature of the ionized

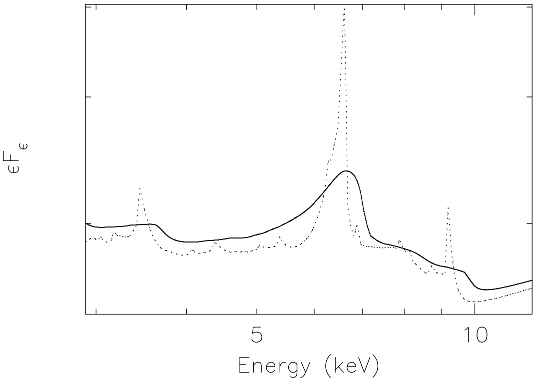

Figure 6. An example of the ionized reflection spectra with (solid line) and without (dotted line) relativistic blurring. This particular example is for the best-fitting model for the 1997 *RXTE* data.

surface layer of the disc (Nayakshin & Kallman 2001), which controls the strength of the spectral features, e.g. iron Kα line emission. The ‘magnetic flare’ geometry, in which the disc is illuminated locally by individual flares (e.g. Haardt, Maraschi & Ghisellini 1997), is used. The power-law source is assumed to have a cut-off energy at 60 keV. The dimensionless accretion rate relative to the Eddington limit is set to 0.5. Fitting the individual spectra yields values ranging from 0.3 to 0.7 for this parameter, but they do not differ significantly from each other within errors. Hence it is fixed at 0.5 in the following fittings. This parameter defines the ionization parameter of the disc, so the above value means that the disc is highly ionized to emit Fe XXV. The inclination (i), inner radius, outer radius and radial emissivity index (α) of the disc are assumed to be $\cos i = 0.9$, $R_{\rm in} = 3R_{\rm S}$, $R_{\rm out} = 100R_{\rm S}$ and $\alpha = 2$, respectively, where $R_{\rm S}$ is the Schwarzschild radius ($= 2r_{\rm g}$). However, $R_{\rm in}$ is allowed to vary in some cases when $3R_{\rm S}$ is found to be outside the 90 per cent confidence limit (for *RXTE*97, *RXTE*98 and *XMM–Newton*). This parameter is chosen to control the strength of relativistic broadening, but it should be noted that the value obtained from the fit does not necessarily mean the true inner boundary of the disc, as it is coupled with the other parameters such as the emissivity index, which is not known. The disc gas is assumed to have solar metallicity. The results of spectral fitting are shown in Table 3 and Fig. 7. The ionized reflection models reproduce the complex spectral features seen in the observed data well, including the strengths of Fe Kα and S XVI RRC.

As we found with the Gaussian fits (Table 2 and Fig. 4b), the iron line flux appears to correlate with the continuum flux, but the *ASCA*93 data show a strong line despite the low continuum flux level, making it an outlier of the correlation. The large EW of the iron line in the *ASCA*93 spectrum is explained by the reflection model with a small value of $l_{\rm X}/l_{\rm d}$, because a cool (temperature of a few hundred eV) layer producing Fe XXV becomes larger in this condition. The plot of $l_{\rm X}/l_{\rm d}$ against iron Kα line EW (Fig. 8) shows this trend; that is, in general, small EW is associated with large $l_{\rm X}/l_{\rm d}$, and vice versa.

3.8 Iron line variability in the long *ASCA* observation

The large EW of the Fe Kα observed in the one-day *ASCA* observation in 1993 may not be a very unusual phenomenon. The longer *ASCA* observation in 1997 was examined for iron line variability. The spectrum taken from the last 20 h of the observation suggests that the EW of the iron line could be as large as 615^{+814}_{-304} eV, in

Table 3. Spectral fitting with reflection spectra from a photoionized disc in hydrostatic balance by S. Nayakshin. The ‘magnetic flare’ geometry is chosen. The illuminating power-law source is assumed to have a high-energy cut-off at 60 keV and variable photon index Γ. The dimensionless accretion rate (relative to the Eddington limit) is set at 0.5. The inclination angle (i), inner radius ($R_{\rm in}$), outer radius ($R_{\rm out}$) and radial emissivity index (α; emissivity $\propto r^{-\alpha}$) of the accretion disc are assumed to be $\cos i = 0.9$, $R_{\rm in} = 3R_{\rm S}$, $R_{\rm out} = 100R_{\rm S}$ and $\alpha = 2$, respectively, for all spectra apart from the two *RXTE* and *XMM–Newton* data sets, for which $R_{\rm in} = 3R_{\rm S}$ was found to be outside the 90 per cent confidence limit and allowed to vary. $R_{\rm S}$ is the Schwarzschild radius ($=2r_{\rm g}$). The metallicity of the disc material is assumed to be the solar value. Relativistic blurring for the Schwarzschild metric (Fabian et al. 1989) is applied. The luminosity ratio of the X-ray illuminating source and thermal emission from the disc, $l_{\rm X}/l_{\rm d}$, is left as the only free parameter in the ionized disc model. A sum of the illuminating power law and reflection, which is absorbed by a cold absorbing column $N_{\rm H}$, is compared with the data. The energy band used for the spectral fittings in each data set is as the same as that is given in Table 2.

Data	Γ	$N_{\rm H}$ (10^{22} cm^{-2})	$l_{\rm X}/l_{\rm d}$	$R_{\rm in}$ ($R_{\rm S}$)	χ^2/d.o.f.
Ginga	$2.20^{+0.08}_{-0.06}$	$1.65^{+0.25}_{-0.21}$	$\leqslant 0.64$	3	12.5/23
*ASCA*93	$2.17^{+0.09}_{-0.11}$	$1.69^{+0.28}_{-0.35}$	$0.08^{+0.13}_{-0.05}$	3	423.8/420
*ASCA*97	$1.96^{+0.05}_{-0.04}$	$1.20^{+0.05}_{-0.05}$	$1.0^{+0.4}_{-0.4}$	3	1867.6/1804
*RXTE*97	$2.28^{+0.03}_{-0.04}$	$3.00^{+0.22}_{-0.30}$	$0.35^{+0.21}_{-0.14}$	18^{+5}_{-8}	48.6/31
*RXTE*98	$2.21^{+0.04}_{-0.05}$	$2.36^{+0.22}_{-0.34}$	$\leqslant 0.2$	34^{+21}_{-9}	39.9/31
BeppoSAX	$2.16^{+0.08}_{-0.06}$	$1.68^{+0.24}_{-0.22}$	$1.0^{+1.0}_{-0.6}$	3	76.8/66
XMM	$2.03^{+0.03}_{-0.01}$	$1.36^{+0.08}_{-0.05}$	$0.28^{+0.19}_{-0.10}$	19^{+26}_{-5}	1130.4/1126

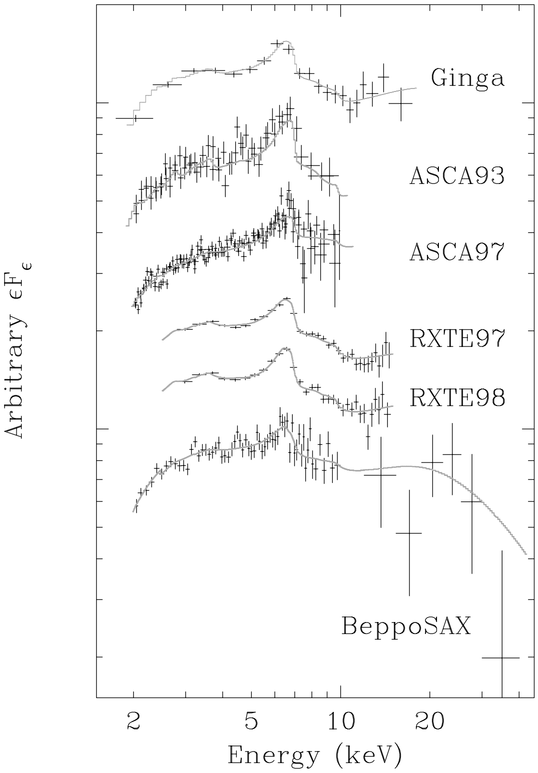

Figure 7. Spectra fitted with ionized reflection model (as shown in thick grey solid lines). The data are shifted along y-axis for clarity and plotted in chronological order (top to bottom for old to new).

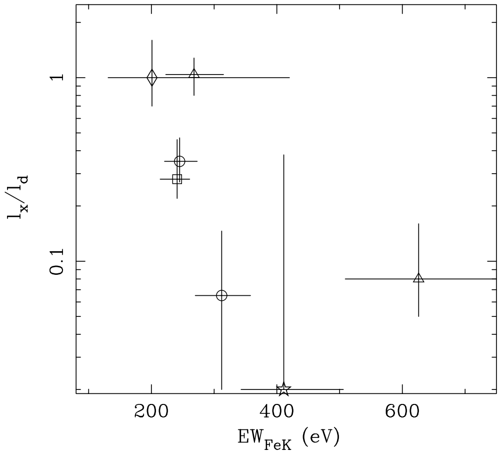

Figure 8. The l_X/l_d parameter in the ionized reflection model fits against Fe Kα line equivalent width obtained from Gaussian fits. Symbols are as in Fig. 4. Error bars represent 1σ errors.

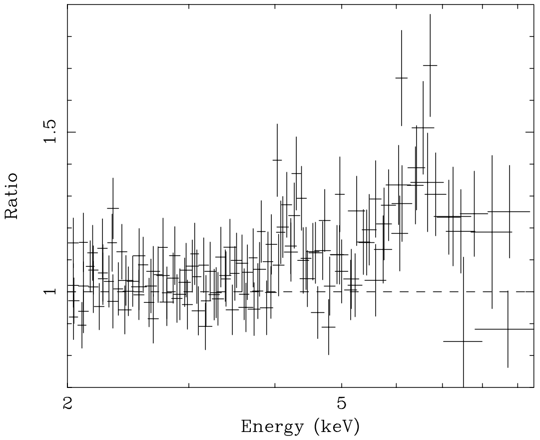

Figure 9. The Fe Kα line profile obtained from the last 20 h of the 1997 *ASCA* observation (the exposure time is ∼28 ks). The data are from the four detectors and are plotted in the form of a ratio to the best-fitting power-law continuum ($\Gamma = 2.04^{+0.20}_{-0.15}$, $N_H = 1.16^{+0.56}_{-0.36}$ cm^{-2}). The line at around 6.5 keV is as strong as the 1993 *ASCA* line profile (Fig. 5). The EW is about 600 eV. Note also another line-like feature at 4.3 keV (see text for details).

contrast to the mean value ∼270 eV (Table 2). During this time interval, two flares were observed to show large amplitudes (a factor of ∼2, see fig. 1 in Iwasawa et al. 1998), but the mean flux 1.83×10^{-11} erg cm^{-2} s^{-1} is slightly below the average of the whole observation (see Table 1).

A significant line-like feature is also detected at an energy of $4.27^{+0.10}_{-0.10}$ keV. The energy is close to that of the Ar XVIII RRC, but the observed strength ($\mathrm{EW} = 94^{+71}_{-48}$) is too large to be identified with that feature. A possible alternative is part of a gravitationally redshifted iron Kα emission, if the line-emitting region is confined to a narrow ring at radius of $\sim 3R_S$ of a nearly face-on disc, which would produce a red horn at that energy range. Fe Kα emission propagating inward after a large flash of X-ray illumination (reverberation) could produce such a feature, although the narrowness of the feature (Gaussian dispersion, $\sigma = 0.17^{+0.19}_{-0.14}$ keV) is not compatible with this interpretation, as it should move across the energy band in a much shorter time-scale (1000 s or less, Young & Reynolds 2000) for the likely black hole mass of this object $\sim 10^7$ M$_\odot$. Another interpretation is substructure in the line profile due to turbulence in a magnetized disc (Armitage & Reynolds 2003), which could account for the 5.6 keV line observed in the spectrum of NGC 3516 (Turner et al. 2002).

We point out that a similar feature, albeit at slightly higher energy of $4.68^{+0.13}_{-0.10}$ keV, is seen in the *ASCA*93 spectrum (see Fig. 5), which also exhibits a large Fe Kα EW. The 4.68 keV feature is unresolved (the 90 per cent upper limit for Gaussian dispersion is $\sigma = 0.22$ keV) and has a line flux of $2.36^{+1.05}_{-1.23} \times 10^{-5}$ photon s^{-1} cm^{-2} (EW $\simeq$ 93 eV).

The ionized reflection model (with the same parameter settings as the fits shown in Table 3 with the addition of a Gaussian for the 4.3 keV line) gives $l_X/l_d = 0.1$ ($\leqslant 0.4$) with $\chi^2 = 742.7$ for 790 degrees of freedom. The small l_X/l_d value is in disagreement with that for the mean spectrum but similar to that of the *ASCA*93 data, suggesting that the accretion disc, as a reflecting medium, might be in a similar state in the two occasions. The fact that the averaged flux for the time interval during which the iron line in Fig. 9 was observed differs very little from that of the rest of the observation implies that the physical condition of the reflector cannot be defined by an averaged source luminosity alone. There might be some other factors that escape our observation.

4 DISCUSSION

We have presented X-ray spectral evidence for highly photoionized matter (Fe Kα and S XVI RRC) in IRAS 18325−5926 and demonstrated that its X-ray spectrum agrees well with a model including reflection from an ionized accretion disc. Relativistic blurring provides a good explanation for the broad spectral features, particularly the iron Kα line, as expected at the inner radius of the accretion disc around a central black hole. We have also tested for a Gaussian smearing of the ionized reflection features. The χ^2 values obtained for the spectral fits favour relativistic blurring over Gaussian smearing for all seven data sets. This indicates that the redward asymmetry, characteristic of the relativistic effects, fits the data better than the symmetric broadening.

A strong iron line from Fe XXV as observed in IRAS 18325−5926 is not very common among Seyfert galaxies. In the particular model for ionized discs illuminated by an X-ray source by Nayakshin et al. (2000), the importance of the thermal structure of the discs is emphasized for a strong ionized iron line to be seen in the observed spectrum. The necessary conditions to create a relatively cool layer of photoionized gas, which emits Fe XXV and Fe XXVI, are met by steep X-ray continuum slope $\Gamma \simeq 2.2$ and a possible continuum roll-over at around 30 keV in IRAS 18325−5926.

We remain cautious about the reality of the continuum roll-over, however. An immediate implication of the high-energy continuum roll-over is that the temperature of the corona above the disc, which Comptonizes soft photons, is cooler than that in other Seyfert galaxies where the cut-off energy is ∼200 keV (e.g. Perola et al. 2002; Malizia et al. 2003). For a photon index of $\Gamma = 2.2$ and $kT_e =$ 30 keV, the optical depth of the corona to Thomson (electron) scattering is $\tau_{es} \simeq 1.7$ (e.g. Beloborodov 1999). If reflection from the disc passes through the corona before reaching an observer, the spectrum of the reflection would be modified greatly through Compton scatterings. This situation can be avoided by the lamp-post type of illumination geometry, where the illuminating source is centrally concentrated above the disc. However, in geometries with magnetized flares occurring in a corona just above the disc, the spectral distortion via Compton scattering is inevitable. For $kT_e \sim 30$ keV, the average fractional photon energy shift per scattering is ∼23 per cent. With $\tau_{\rm es} = 1.7$, a large fraction of photons from the disc would be scattered $N = 2$–3 times and double their energy, by a factor of $\exp[N(4kT_{\rm e}/m_{\rm e}c^2)]$, where $N \sim \tau_{\rm es}^2$ (Rybicki & Lightman 1979). Expected effects on the observed spectrum are broadened spectral features and reduction of the iron line EW by more than half (e.g. Petrucci et al. 2001). The Fe Kα line profile would be broadened significantly with $\sigma > 1$ keV and skewed to higher energies (e.g. Pozdnyakov, Sobol & Sunyaev 1979).

The fact that we sometimes observe a high EW of Fe Kα as large as 600 keV does not support the view that the reflection emission undergoes significant Comptonization within the corona. If the EW of Fe Kα was controlled by the optical depth of the corona, then an anticorrelation between linewidth and EW of Fe Kα would be expected, which is however not observed (see Table 2). The redward asymmetry of the spectral features due to relativistic blurring, which fits data well as mentioned above, is inconsistent with the expected line profile emerging from the optically thick Comptonizing corona. These would constrain the disc illumination geometry to a limited type such as the lamp-post model (the patchy corona model may work as well, since a fair fraction of the disc surface is left uncovered by the corona), if the 30 keV roll-over is real. When a source is variable, localized illumination of the disc expected in the patchy corona model would lead to the reflected spectrum behaving differently from that in the lamp-post model, e.g. a significant contribution from low ionization reflection could be present, as discussed by Collin et al. (2003). Given the presence of relativistic broadening, this is hard to examine with the iron line emission. No significant cold reflection is required by the high-energy continuum observed with *Ginga*, *RXTE* and *BeppoSAX*, although weak 6.4 keV line emission is seen in the high-quality *XMM–Newton* data.

The cool corona would mean that the production of high-energy photons via Compton up-scattering needs more scatterings, resulting in longer delay of hard X-ray emission relative to softer X-ray emission, which might be the case for the energy dependence of the X-ray light curves obtained from the *XMM–Newton* observation (Iwasawa et al., in preparation). Therefore, given the implications mentioned above, verifying the roll-over is highly desirable. It will probably have to wait until the launch of *ASTRO-E2*.

Among the seven recent X-ray observations presented in this paper, spanning over 12 yr, the iron line flux has changed significantly in response to the continuum change. The line flux appears to correlate with the continuum flux in at least some cases, but the strength of the line may be determined in a more complex way (e.g. Nayakshin & Kazanas 2002; Collin et al. 2003), as the presence of occasional outliers suggests (see also discussion in Section 3.8). The accretion rate, the disc illumination pattern, the physical conditions of the X-ray emitting corona and the ionized surface of the disc, and also strong relativistic effects (Cunningham 1976; Martocchia & Matt 1996; Miniutti et al. 2003) may all play a role in controlling the production of the iron line emission. As shown in Fig. 8, the temperature of the disc surfaces inferred from $l_{\rm X}/l_{\rm d}$ may be important. This parameter could be related to the fraction of accretion power going into the corona, which changes in time. Further complexity is added by the time dependence of some of those properties mentioned above. Since rapid variability is common in this source (see e.g. Fig. 1), the X-ray source is unlikely to be in a steady state. In this paper, we have investigated data averaged over the durations of half to a few days, for which the time evolution in heating and cooling of the Comptonizing corona (e.g. Guilbert, Fabian & Ross 1982) should be averaged over each observed duration, whilst the dynamical time-scale of the accretion flow is perhaps relevant. The unusually large EW of the line appears only in relatively short time intervals ($\leqslant$1 d) as discussed in Section 3.8, which may be intriguing in this respect.

In the presence of strong reflection from a highly ionized disc, nearly half of the observed X-ray flux, e.g. in the 2–10 keV band, is attributed to the reflection. This would reduce the estimate of the intrinsic luminosity of the illuminating X-ray source by approximately half.

ACKNOWLEDGMENTS

Sergei Nayakshin and Matteo Guainazzi are thanked for useful discussions. ACF and KI acknowledge the Royal Society and PPARC, respectively, for support. AJY and CSR acknowledge support from NASA grant NAG5-9935 and the National Science Foundation grant AST0205990, respectively. JCL acknowledges support from the Chandra Fellowship grant PF2-30023 – this is issued by the Chandra X-ray Observatory Center, which is operated by SAO for and on behalf of NASA under contract NAS8-39073.

REFERENCES

Armitage P. J., Reynolds C. S., 2003, MNRAS, 341, 1041
Awaki H., Koyama K., Inoue H., Halpern J. P., 1991, PASJ, 43, 195
Ballantyne D. R., Iwasawa K., Fabian A. C., 2001a, MNRAS, 323, 506
Ballantyne D. R., Ross R. R., Fabian A. C., 2001b, MNRAS, 327, 10
Barrio F. E., Done C., Nayakshin S., 2003, MNRAS, 342, 557
Beloborodov A. M., 1999, in Poutanen J., Svensson R., eds, ASP Conf. Ser. Vol. 161, High Energy Processes in Accreting Black Holes. Astron. Soc. Pac., San Francisco, p. 295
Carter D., 1984, Astron. Express, 1, 61
Collin S., Coupé S., Dumont A.-M., Petrucci P.-O., Rózanska A., 2003, A&A, 400, 437
Comastri A. et al., 1998, A&A, 333, 31
Cunningham C., 1976, ApJ, 208, 534
De Grijp M. H. K., Miley G. K., Lub J., DeJong T., 1985, Nat, 314, 240
Dickey J. M., Lockman F. J., 1990, ARA&A, 28, 215
Fabian A. C., Vaughan S., 2003, MNRAS, 340, L28
Fabian A. C., Rees M. J., Stella L., White N. E., 1989, MNRAS, 238, 729
George I. M., Fabian A. C., 1991, MNRAS, 249, 352
Guilbert P. W., Fabian A. C., Ross R. R., 1982, MNRAS, 199, 763
Haardt F., Maraschi L., Ghisellini G., 1997, ApJ, 476, 620
Iwasawa K., Kunieda H., Tawara Y., Awaki H., Koyama K., Murayama T., Taniguchi Y., 1995, AJ, 110, 551
Iwasawa K., Fabian A. C., Mushotzky R. F., Brandt W. N., Awaki H., Kunieda H., 1996a, MNRAS, 279, 837
Iwasawa K. et al., 1996b, MNRAS, 282, 1038
Iwasawa K., Fabian A. C., Brandt W. N., Kunieda H., Misaki K., Terashima Y., Reynolds C. S., 1998, MNRAS, 295, L20
Iwasawa K., Fabian A. C., Young A. J., Inoue H., Matsumoto C., 1999, MNRAS, 306, L19
Kojima Y., 1991, MNRAS, 250, 629
Laor A., 1991, ApJ, 376, 90
Lee J. C., Fabian A. C., Brandt W. N., Reynolds C. S., Iwasawa K., 1999, MNRAS, 310, 973
Leighly K., 1999, ApJS, 125, 297
Malizia A., Bassani L., Stephen J. B., Di Cocco G., 2003, ApJ, 589, L17
Martocchia A., Matt G., 1996, MNRAS, 282, L53
Matsuoka M., Piro L., Yamauchi M., Murakami T., 1990, ApJ, 361, 440
Matt G., Fabian A. C., Ross R. R., 1993, MNRAS, 262, 179
Miniutti G., Fabian A. C., Goyder R., Lasenby A. N., 2003, MNRAS, 344, L17
Nandra K., Pounds K. A., 1994, MNRAS, 268, 405
Nandra K., Mushotzky R. F., Yaqoob T., George I. M., Turner T. J., 1997a, MNRAS, 284, L7
Nandra K., George I. M., Mushotzky R. F., Turner T. J., Yaqoob T., 1997b, ApJ, 477, 602

Nandra K., George I. M., Mushotzky R. F., Turner T. J., Yaqoob T., 1997c, ApJ, 488, L91
Nayakshin S., Kallman T. R., 2001, ApJ, 546, 406
Nayakshin S., Kazanas D., 2002, ApJ, 567, 85
Nayakshin S., Kazanas D., Kallman T. R., 2000, ApJ, 537, 833
Perola G. C., Matt G., Cappi M., Fiore F., Guainazzi M., Maraschi L., Petrucci P. O., Piro L., 2002, A&A, 389, 802
Petrucci P. O., Merloni A., Fabian A., Haardt F., Gallo E., 2001, MNRAS, 328, 501
Petrucci P. O. et al., 2002, A&A, 388, L5
Piccinotti G., Mushotzky R. F., Boldt E. A., Holt S. S., Marshall F. E., Serlemitsos P. J., Shafer R. A., 1982, ApJ, 253, 485
Pounds K. A., Nandra K., Stewart G. C., George I. M., Fabian A. C., 1990, Nat, 344, 132
Poutanen J., Svensson R., 1996, ApJ, 470, 249
Pozdnyakov L. A., Sobol I. M., Sunyaev R. A., 1979, A&A, 75, 214
Ross R. R., Fabian A. C., 1993, MNRAS, 261, 74
Ross R. R., Fabian A. C., Young A. J., 1999, MNRAS, 306, 461
Rybicki G. B., Lightman A. P., 1979, Radiation Processes in Astrophysics. Wiley-Interscience, New York
Shih D. C., Iwasawa K., Fabian A. C., 2002, MNRAS, 333, 687
Smith D. A., Done C., 1996, MNRAS, 280, 355
Stern B. E., Poutanen J., Svensson R., Sikora M., Begelman M. C., 1995, ApJ, 449, L13
Tanaka Y. et al., 1995, Nat, 375, 659
Turner T. J. et al., 2002, ApJ, 574, L123
Vaughan S., Boller Th., Fabian A. C., Ballantyne D. R., Brandt W. N., Trümper J., 2002, MNRAS, 337, 247
Ward M. J., Done C., Fabian A. C., Tennant A. F., Shafer R. A., 1988, ApJ, 324, 767
Weaver K. A., Reynolds C. S., 1998, ApJ, 503, L39
Yaqoob T., Serlemitsos P. J., Turner T. J., George I. M., Nandra K., 1996, ApJ, 470, L27
Young A. J., Reynolds C. S., 2000, ApJ, 529, 101

This paper has been typeset from a TEX/LATEX file prepared by the author.